Energy flow of λ in Hořava-Lifshitz cosmology

Ewa Czuchry[1,*] and Nils A. Nilsson[2,3,†]

[1]*Institute of Mathematics and Cryptology, Military University of Technology, ul. gen. Sylwestra Kaliskiego 2, 00-908 Warszawa 46, Poland*

[2]*Cosmology, Gravity and Astroparticle Physics Group, Center for Theoretical Physics of the Universe, Institute for Basic Science, Daejeon 34126, Korea*

[3]*SYRTE, Observatoire de Paris, Université PSL, CNRS, LNE, Sorbonne Université, 61 avenue de l'Observatoire, 75 014 Paris, France*

(Received 27 April 2023; accepted 8 May 2024; published 2 August 2024)

Hořava-Lifshitz gravity has been proposed as a renormalizable and ghost-free quantum gravity model candidate with an anisotropic UV-scaling between space and time. We present here a cosmological background analysis of two different formulations of the theory, with particular focus on the running of the parameter λ. Using a large dataset consisting of cosmic microwave background data from *Planck*, Pantheon + supernovae catalog, SH0ES Cepheid variable stars, baryon acoustic oscillations (BAO), cosmic chronometers, and gamma-ray bursts (GRB), we arrive at new bounds on the cosmological parameters, in particular λ, which runs logarithmically with energy and describes deviation from general relativity, which corresponds to $\lambda = 1$ For the detailed balance scenario we arrive at the bound $\lambda = 1.0406 \pm 0.0023$, and for beyond detailed balance the limit reads $\lambda = 1.0064 \pm 0.0002$. We also study the influence of different datasets and priors, and we find that removing low-redshift data generally moves λ closer toward UV values, while simultaneously widening the error bars. In the detailed balance scenario, this effect is more noticeable, and without prior $\lambda \geq 1$ it takes on values that are significantly below unity.

DOI: 10.1103/PhysRevD.110.043502

I. INTRODUCTION

General relativity (GR), one of the most successful physical theories, is widely known to be nonrenormalizable; therefore, its application to very small distances and high energies, such as at the very early Universe is expected to be inconsistent. In light of this, a different theory of gravity was recently proposed by Hořava [1] in order to capture the quantum effects of the gravitational field in the early stages of the Universe. This theory is a fascinating proposal of modified gravity equipped with an anisotropic scaling at the Planck scale given in term of a critical Lifshitz exponent which contributed to the name Hořava-Lifshitz (HL) gravity. This Lifshitz scaling in the ultraviolet (UV) regime inevitably breaks Lorentz invariance explicitly.[1]

By giving up on the idea of invariance under four-dimensional diffeomorphisms, it becomes possible to add higher order spatial-derivative terms to the Lagrangian without including higher-order time derivatives. Therefore, one avoids the Ostrogradzky ghosts compromising unitarity of the corresponding quantum theory. The resulting Lagrangian is invariant under three-dimensional spatial diffeomorphisms only, but the theory becomes renormalizable at high energies. Due to the explicit lack of invariance under four-dimensional diffeomorphisms, the HL theory is naturally expressed using the Arnowitt-Deser-Misner (ADM) 3 + 1 formulation [3].

The most straightforward option for a group which can accommodate this property is the set of foliation-preserving diffeomorphisms which includes time reparametrizations and three-dimensional spatial diffeomorphisms. Under this symmetry group, the kinetic term of the action acquires an additional coupling denoted by λ. In GR, there is no need for that coupling as the very specific linear combination of curvature terms contained within the classical Hilbert-Einstein action remains unchanged under general four-dimensional diffeomorphisms. In HL theory, the limit $\lambda \to 1$ is supposed to recover GR, which should in theory provide its low-energy limit in a straightforward manner, but achieving this limit presents some issues. One one

*ewa.czuchry@wat.edu.pl

†nilsson@ibs.re.kr

[1]See for example [2] for a discussion of explicit and spontaneous symmetry-breaking in gravity.

hand, the critical Lifshitz exponent z and the $(3+1)$-foliation parameter λ are the parameters of HL theory, where λ is also associated with a restricted foliation corresponding to $z=1$ in the Lifshitz scaling. As z approaches unity in the low-energy limit, it is also necessary that $\lambda \to 1$ and consequently that Lorentz invariance is restored. Additionally, the familiar ADM foliation of GR is also recovered. Because the coupling constant λ disrupts the general covariance in the presence of spacetime diffeomorphisms, it is thought that values of λ different from 1 will cause the model to deviate from GR.

On the other hand, due to the reduced symmetry, the action of HL gravity [1] differs from the classical Einstein-Hilbert action even in the infrared limit, where only terms up to second order in spatial derivatives are considered. Even though the IR limit differs from GR, it is supposed that one can still obtain it as an approximate solution at long distances; however, it seems that this connection with GR is problematic, since in order to obtain it, it is necessary to disregard the higher order derivative terms in the action. Additionally, the GR limit presents issues because HL contains an extra degree of freedom present as a scalar graviton, which causes a significant challenge in terms of the credibility of the theory [4–8].

The first minimum formulation (also called the Hořava toy model) was based on two conditions which minimised the number of terms in the action, which are

(1) *The detailed balance condition*, which limits the potential part of the action only to terms which may be derived from a superpotential, and
(2) *The projectability condition*, which assumes that the lapse function N depends only on time $N=N(t)$.

In spite of its simplicity, this formulation from a lot of problems and inconsistencies (see e.g., [4,9,10]) like the existence of a parity violating term [4], wrong sign and very large value of the cosmological constant [11,12], ghost instabilities and problems with strong coupling at very low energies [7,13] and problems with power counting renormalization of the scalar mode [14,15]. Relaxing the detailed balance condition in the so-called Sotiriou-Visser-Weinfurtner (SVW) generalization [4] healed some of the initial theory problems and provided a better IR limit, but the resulting theory still enters into the strong coupling regime at low energies, which causes problems with the flow to GR. That might imply that either this formulation is not theoretically valid [9], as it does not have a good GR limit, or that the theory retains Lorentz violation even at low energies but modifications brought by this are small enough to fit the current observational data [8]. It is also possible that flowing to GR requires nonlinear perturbative analysis, as presented in the [16–18] where the IR limit recovers GR with built-in dark matter.

The problematic low-energy limit of the theory led to the formulation of the so-called healthy extension [9] which abandons the projectability condition; in this formulation, the lapse N is a dynamical field that depends on all spacetime coordinates, inducing a large number of additional operators in the action. At low energies, it reduces to a scalar-tensor gravity theory which exhibits deviations from GR. These deviations can be suppressed by an appropriate choice of parameters cosmological constraints on departures from Lorentz symmetry [19] and on preferred time models [20]. Nonetheless, the dynamic lapse element of the metric induces an instantaneous interaction that is problematic in the renormalizability analysis of the theory. On the contrary, the projectable version has been demonstrated to be perturbatively renormalizable [21,22] in a strict sense in all space dimensions. In the context of $2+1$ dimensions, a calculation of its renormalization group (RG) flow was conducted [23], revealing an asymptotically free UV fixed point. This outcome signifies the UV completeness of the $2+1$-formulation. In the case of $3+1$ dimensions, partial results regarding the RG flow of projectable HG were obtained in [22], and a complete set of beta functions for the six crucial couplings was derived in [24], where potential candidates for asymptotically free UV fixed points were found and analyzed. The existence of asymptotically free fixed points suggests that it is possible to treat the problem of strong coupling in the IR in analogy to QCD [23,25]. Therefore, the projectable theory might require using nonperturbative techniques like lattice calculations, in order to fully describe phenomenological aspects of scalar mode decoupling at low energies. The theoretical work on the renormalization aspects of the theory is still being carried out, including on a nonprojectable version. Preliminary results [26] showed that the nonlocal divergences appearing as the result of instantaneous interaction induced by the dynamics of a full lapse field (in the nonprojectable formulation) might be canceled at all orders in the loop expansion; therefore, it seems that both HL gravity versions are worth thorough investigation.

The simpler projectable version is now a realistic quantum gravity model and has other interesting cosmological features which are not provided by a full theory, in spite of its problems at low energies. Namely, it leads naturally to cosmological dark matter [27,28], offers a generation method of producing cosmological perturbations that are scale-invariant, addressing the horizon problem [29] and presents a potential resolution to the flatness problem [30]. In projectable HL gravity, the Hamiltonian constraint is global rather than local, and it is possible that integrating it over the whole space provides an integration constant which in the IR limit behaves like cold dark matter, without the need of adding extra ingredients. Moreover, in the nonprojectable version the local Hamiltonian constraint is enforced at every spatial point within each local universe, therefore not allowing for a global integration constant. Moreover, in quantum cosmology there is the prominent Hartle-Hawking no-boundary proposal, a hypothesis describing the quantum genesis of

the universe from nothing, which has been recently formulated within HL gravity [31]. This formulation involves the utilization of the Lorentzian path integral, which, under certain conditions gives rise to the no-boundary wave function of the universe.

The nonprojectable version has a stable IR limit where it may reproduce GR phenomenology along with that of some remnant of Lorentz violation; this could be used to set observational bounds on the theory in the IR. Black holes within nonprojectable Horava gravity are particularly intriguing as they exhibit a universal trapping surface known as the universal horizon [32,33]. This serves as a causal boundary for trajectories, irrespective of their speed. Significant work has been done on that subject and its consequences in terms of black hole thermodynamics and Hawking radiation [34–36] as well as resolving singularity problems [37]. Other research direction in different formulations of HL gravity include also the black-hole shadow [38,39] and formulations of quantum gravity models [40–46]. Current state of research on Horava gravity with an extensive list of references is contained in the recent reviews [47,48].

Given current theoretical state-of-the-art, it is worth investigating observational implications and parameter bounds of both classes of Horava gravity from the phenomenological point of view. At the moment this theory keeps fulfilling different observational constraints, the tightest coming from the propagation and emission of gravitational waves from compact objects [49], numerical studies of slowly moving binary black-hole solutions [50], and observations of the damping of the period of quasicircular binary pulsars and of the triple system PSR J0337 + 1715 [51]. However, although narrowing the allowed parameter space, these constraints mainly provide bounds on the tensor mode and PPN parameters which quantify preferred-frame effects, leaving other parameters like λ basically unconstrained. This comes from the interesting fact [52] that the dynamics of gravitational collapse and the perturbations of spherically symmetric metrics are indistinguishable from those of GR; similar results were obtained in [50] from slowly moving binary black hole solutions in HL theories. Moreover, theories with asymptotically flat spacetimes different from GR only when $\lambda \neq 1$ (the so-called $\lambda - R$, have been shown to be equivalent to GR [53].

It seems that the most meaningful constraint on λ, a parameter that controls energy flow and in some approaches Lorentz violation, comes from cosmological observations. Indeed, some first rough bounds were obtained from big bang nucleosynthesis (BBN) predictions for primordial abundances, along with constraints on the ratio between the "local" gravitational constant G and the "cosmological" counterpart G_{cosmo}[2] [54], and was further more narrowed from constraints on the quadratic cuscuton mode comparing large scale structure with cosmic microwave background (CMB) data [55]. However, in such approaches all the other parameters of the theory remain constant, and therefore the resulting bounds are rather rough. More general approaches include allowing variations of all model parameters and systematic numerical investigations of constraints from cosmological data, including supernovae type Ia, (SNIa), baryon acoustic oscillations (BAO), and CMB data. The first constraints on λ as well as other parameters of the theory where obtained using such a general approach in [56], reporting $|\lambda - 1| \lesssim 0.02$. Other approaches include exploiting bounds on the Hubble parameter tension by one of us [57], thereby providing bounds $0.95 \leq \lambda \leq 1.16$, and [58] investigated the effects of a λ phase transition in AdS black holes. In the works by one of us [59] and [60], the authors considered a constant λ and reabsorbed it into other parameters.

The observational bounds on the nonprojectable version are more complicated, as this theory implies that the propagation speed of the scalar mode will generically differ from that of the tensor mode, and therefore Lorentz violations are generically present at all energies. In order to be compatible with observational results some parameters have to be tuned to specific ranges. Deviations from Lorentz invariance in the matter sector are strongly constrained as compared to the gravitational sector, allowing a larger region of the parameter space in observational tests [49,51,61]. The work [61] is however based on a flat model, and there is an ongoing discussion on the possible nonzero value of the curvature parameter both in the ΛCDM model [62] and its alternatives, including HL cosmology. The papers [49,51] were mainly based on the propagation and emission of gravitational waves from compact objects which, does not provide good bounds on λ; however, the results of [51] actually seem to favor aether/ khronometric theories over GR (it was shown in [63] that the khronometric model corresponds to the low-energy limit of nonprojectable Hořava gravity). Interesting results were obtained in [64] but this paper required that the Lorentz-violating field be dark energy only, whereas subsequent work [19] concerned Lorentz violation in the dark matter sector, and therefore these results cannot be applicable to the full theory. Both [64] and [19] provided similar bounds on λ as the ones mentioned above.

In this paper we set new bounds on HL parameters, while λ which in in previous studies is set to a constant, is allowed to vary. We also perform a detailed examination regarding how removing low-redshift data impact the obtained bounds on this parameter. An intriguing matter comes to light, whether higher redshift data could push λ further from the classical limit at the value of unity, as would be expected of HL or similar extensions of Einstein gravity (with additional terms in the action). We focus first on a

[2]In general, these two are not the same in theories where Lorentz invariance is broken.

projectable version of HL whose quantum properties are better understood, leaving the nonprojectable version with a larger number of parameters for later studies. In order to be phenomenologically viable we perform our analysis with and without the detailed-balance condition, leaving theoretical considerations favoring the latter model aside, and including different datasets and priors on the value of λ.

This paper is organized as follows: We first give a brief overview of the theory of HL cosmology in both scenarios under consideration. We then go on to describe how we rewrite the equations to allow for numerical analysis. Finally, we present our results and discuss them.

II. HOŘAVA-LIFSHITZ COSMOLOGY

Here we briefly outline the equations governing cosmological evolution in Hořava-Lifshitz gravity [65,66]. For a more in-depth discussion we refer to our recent paper [67], and also to [47].

Hořava-Lifshitz gravity offers the possibility of creating a theory of gravity which remains finite and well defined at high energies, while also reproducing GR in the classical regime. This is achieved by introducing a fixed point in the UV region of the renormalization group, where time and space behave differently under scale transformations. Specifically, the scaling relations at the Planck scale should satisfy $t \to b^{-z}t$, $x^i \to b^{-1}x^i$, $i = 1, 2, 3$, where b is a scaling parameter and z is the critical Lifshitz exponent which characterizes the fixed point. As usual, t stands for time and x^i for spatial coordinates. Different models can be identified by specific choices of z; for a pure gravity theory in d spatial dimensions which is invariant under foliation-preserving diffeomorphisms and is power-counting renormalizable, z must be greater than or equal to d, equivalently in 4-dimensional physical space-time to $z \geq 4$ [47]. In order to restore Lorentz invariance, z needs to be set to unity.

Due to the anisotropic scaling present in the theory, it is useful to write down the metric using the ADM decomposition:

$$ds^2 = -N^2dt^2 + g_{ij}(dx^i + N^i dt)(dx^j + N^j dt), \quad (1)$$

where N and N^j are the lapse function and shift vector, respectively, and g_{ij} is the spatial metric $(i, j = 1, 2, 3)$. Given this, we can express the most general form of the theory as:

$$S = \int d^3x dt N\sqrt{g}[K^{ij}K_{ij} - \lambda K^2 - \mathcal{V}(g_{ij})], \quad (2)$$

where g is the determinant of the spatial metric, λ is the running coupling and $\mathcal{V}$ is a potential. K_{ij} represents the extrinsic curvature. The potential term contains only dimension 4 and 6 operators which can be constructed from the spatial metric g_{ij}. The square $K^{ij}K_{ij}$ and its trace-squared K^2 are individually invariant under the reduced symmetry group, however for $\lambda = 1$ the full kinetic term $K^{ij}K_{ij} - K^2$ acquires invariance under four-diffeomorphisms.

A. Detailed balance (DB)

The detailed-balance condition is a way to reduce the number of terms in the action (2) by assuming that it should be possible to derive $\mathcal{V}$ from a superpotential W [11,68]:

$$\mathcal{V} = E^{ij}\mathcal{G}_{ijkl}E^{kl}, \qquad E^{ij} = \frac{1}{\sqrt{g}}\frac{\delta W}{\delta g_{ij}},$$
$$\mathcal{G}^{ijkl} = \frac{1}{2}(g^{ik}g^{jl} + g^{il}g^{jk}) - \lambda g^{ij}g^{kl}. \quad (3)$$

which for $\lambda = 1$ reduces to the standard Wheeler-DeWitt metric. From this the most general action can be written as:

$$S_{db} = \int \mathrm{d}^3x\mathrm{d}t\sqrt{g}N\left[\frac{2}{\kappa^2}(K_{ij}K^{ij} - \lambda K^2) + \frac{\kappa^2}{2\omega^4}C_{ij}C^{ij}\right.$$
$$- \frac{\kappa^2\mu}{2\omega^2}\frac{\epsilon^{ijk}}{\sqrt{g}}R_{il}\nabla_j R^l_k \quad (4)$$
$$\left. + \frac{\kappa^2\mu^2}{8}R_{ij}R^{ij} + \frac{\kappa^2\mu^2}{8(1-3\lambda)}\left(\frac{1-4\lambda}{4}R^2 + \Lambda R - 3\Lambda^2\right)\right], \quad (5)$$

where C^{ij} is the Cotton tensor, ϵ^{ijk} is the totally antisymmetric tensor, and the parameters κ, ω, and μ have mass dimension -1,0, and 1, respectively. This action has been obtained from (2) by analytic continuation of the parameters $\mu \mapsto i\mu$ and $\omega^2 \mapsto -i\omega^2$, which enables positive values of the bare cosmological constant Λ, which does not happen in the original formulation. The coupling constant λ runs with energy logarithmically. The reduced symmetry of the action (compared to GR), induces propagation of an extra scalar degree of freedom, which has a positive-definite kinetic term in the UV for $G > 0$ and $\lambda \in (-\infty, 1/3) \cup (1, \infty)$, therefore enabling ghost-free and unitary formulation of the corresponding quantum theory. However, this mode seems to exhibit pathological behavior when approaching the limit $\lambda \to 1$, thereby losing perturbative stability [4–8]. This can be cured by fine tuning of λ (set to 1 up to 10^{-61}) or by expanding around a curved vacuum, which still does not provide stable Minkowski limit. Other results [16–18] show that if $\lambda \to 1$ fast enough, the projectable theory converts to GR in a way similar to the Vainshtein mechanism whereas the scalar mode IR instability gets restrained [16]. Another possible mechanism to address the problems of instabilities and strong coupling of the scalar graviton is its condensation via a phase transition analogous to the one in QCD [8,25]. Therefore, it seems the only relevant scenario which permits a potential renormalization flow toward general relativity (at $\lambda = 1$) is when

$\lambda \geq 1$, as the region for values of λ less than or equal to $1/3$ is separated by a problematic interval $1/3 < \lambda < 1$ in which a quantum version is not unitary due to existence of gravitons with negative-definite kinetic terms in the UV. RG flow calculated in $2+1$ dimensions exhibits a UV attractive and asymptotically free fixed point at $\lambda = 15/14$ as well as the flow $\lambda \to 1^+$ in the IR. Another UV fixed point is $\lambda = 1/2$, and also quite counterintuitive IR flow $\lambda \to \infty$. The structure of the propagators and vertices in $3+1$ dimensions is significantly more complicated than in $2+1$ dimensions, providing at the moment only partial results on the RG flow via studies of β-functions for G and λ ([22]) as well as for the remaining independent couplings [24]. The results of the latter work do not seem to exhibit any asymptotically free fixed points for finite values of λ in the interval $\lambda \in (1, \infty)$, but shows four asymptotically fixed but UV repulsive points along the λ-direction in the other unitary interval $\lambda \in (0, 1/3)$. It is not yet known if they are attractive or not along the other directions. The earlier paper [69] proposed a UV point $\lambda \to \infty$ (which in $2+1$ dimensions represented an IR point), that seemed to be stable and resulted in nonsingular equations of motion at the classical level. Therefore, the paper [24] also analyses that limit while identifying eight fixed points with three o them being both UV attractive and asymptotically free. The full structure of the RG flow is not yet fully known, and he existence of a finite and asymptotically free UV fixed point in the region $\lambda \in (1, \infty)$ is neither excluded nor yet found.

As the present paper is a *phenomenological* one, we *have not imposed any condition on* λ and let it be as free as possible. The idea is that certain formulations of HL gravity may be ruled out by the model preferring unphysical values of λ when confronted with data. For completeness, we also investigate the case when $\lambda \geq 1$. However, in the initial numerical results, we noted that while λ does indeed take on values smaller than unity, it never gets close to $1/3$ (which is parameter singularity), and we therefore introduced the $\lambda > 1/3$ prior to save computation time, without loss of generality. There is a theoretical possibility [24] of the existence of UV fixed points in the region $\lambda < 1/3$, but this is unreachable with current data, which lies far from the true UV regions.

We populate our model with the canonical matter and radiation fields represented by the energy densities (and pressures) ρ_m (p_m) and ρ_r (p_r), both of which are subject to the continuity equation $\dot{\rho} + 3H(\rho + p) = 0$. Here, an overdot represents a time derivative. Moreover, we use the projectability condition [68] $N = N(t)$, and we use the standard FLRW line element $g_{ij} = a(t)^2 \gamma_{ij}$, $N^i = 0$, where γ_{ij} is the maximally symmetric constant curvature metric. It is important to remember that in theories which violate Lorentz symmetry the gravitational constant appearing in the gravitational action $G_{\rm grav}$ generally does *not* coincide with the one which appears in the Friedmann equations, $G_{\rm cosmo}$ [56,70]. This could in principle be used to set bounds on λ (as was done in [57]), but we will not adopt this approach in this paper.

Varying the action (4) with respect to N and a we arrive at the Friedmann equations for the detailed balance scenario:

$$\left(\frac{\dot{a}}{a}\right)^2 = \frac{\kappa^2}{6(3\lambda-1)}[\rho_m + \rho_r] + \frac{\kappa^2}{6(3\lambda-1)}\left[\frac{3\kappa^2\mu^2K^2}{8(3\lambda-1)a^4} + \frac{3\kappa^2\mu^2\Lambda^2}{8(3\lambda-1)}\right] + \frac{\kappa^4\mu^2\Lambda K}{8(3\lambda-1)^2a^2}, \tag{6}$$

$$\frac{\mathrm{d}}{\mathrm{d}t}\frac{\dot{a}}{a} + \frac{3}{2}\left(\frac{\dot{a}}{a}\right)^2 = -\frac{\kappa^2}{4(3\lambda-1)}[p_m + p_r] - \frac{\kappa^2}{4(3\lambda-1)}\left[\frac{\kappa^2\mu^2K^2}{8(3\lambda-1)a^4} - \frac{3\kappa^2\mu^2\Lambda^2}{8(3\lambda-1)}\right] - \frac{\kappa^4\mu^2\Lambda K}{16(3\lambda-1)^2a^2}. \tag{7}$$

We can therefore define $G_{\rm cosmo} = \kappa^2/(3\lambda-1)$ and $\kappa^4\mu^2\Lambda = 8(3\lambda-1)^2$ by requiring that (6), (7) coincide with the standard Friedmann equations. Clearly, when Lorentz invariance is restored, λ is set to unity and $G_{\rm grav} = G_{\rm cosmo}$. Under detailed balance, and using the units $8\pi G_{\rm grav} = 1$, we are lead to $\kappa^2 = 4$, $\mu^2\Lambda = 2$, and by introducing the standard density parameters we arrive at the Friedmann equation suitable for our analysis:

$$H^2 = H_0^2\left[\frac{2}{3\lambda-1}\left(\Omega_{m0}(1+z)^3 + \Omega_{r0}(1+z^4)\right) + \Omega_{K0}(1+z)^2 + \omega + \frac{\Omega_{K0}^2}{4\omega}(1+z)^4\right] \tag{8}$$

where H denotes the Hubble parameter and the subscript 0 indicates the value as measured today. We have also introduced a parameter $\omega = \Lambda/(2H_0^2)$.[3] A characteristic feature of HL theory is the appearance of a dark radiation term in (8): $\Omega_{k0}^2/4\omega$, and we can express this in terms of the effective number of neutrino species $\Delta N_{\rm eff}$ present during the BBN epoque (See Refs. [56,67,71]) as $\Omega_{k0}^2/4\omega = 0.13424\Delta N_{\rm eff}\Omega_{r0}$. We can also obtain a constraint from the $z = 0$ limit, where $H|_{z=0} = H_0$, which reads: $(1 - \Omega_{k0} - \omega - \Omega_{k0}^2/(4\omega))(3\lambda-1)/2 = \Omega_{m0} + \Omega_{r0}$. We abbreviate the detailed balance case as DB.

B. Beyond detailed balance (BDB)

There has been an ongoing discussion in the literature whether the detailed balance condition is too restrictive [47,65,66], or if relaxing it can cure the theory from the quantum instabilities of the scalar mode [6,9,72–74]. On

[3]Which is not to be confused with the IR-modification parameter, which is usually also denoted by ω.

one hand the detailed-balance condition introduces a superpotential, which might simplify the quantization process significantly; on the other hand, this condition is not fundamental, but helps in, e.g., reducing the number of independent couplings in the theory.

Therefore, we may safely consider the Sotiriou-Visser-Weinfurtner (SVW) [4] generalization with this condition relaxed, after which the potential $\mathcal{V}$ contains additional terms. In this scenario the action includes quantities not only up to quadratic in curvature, as in the original HL formulation, but also cubic ones, while suppressing parity violating terms. Applying the generalized action to the maximally symmetric constant curvature metric results in the following analog of the Friedmann equations [10,13]:

$$\left(\frac{\dot{a}}{a}\right)^2 = \frac{2\sigma_0}{3\lambda-1}(\rho_m+\rho_r) + \frac{2}{3\lambda-1}\left[\frac{\Lambda}{2} + \frac{\sigma_3 K^2}{6a^4} + \frac{\sigma_4 K}{6a^6}\right] + \frac{\sigma_2}{3(3\lambda-1)}\frac{K}{a^2}, \tag{9}$$

$$\frac{\mathrm{d}}{\mathrm{d}t}\frac{\dot{a}}{a} + \frac{3}{2}\left(\frac{\dot{a}}{a}\right)^2 = -\frac{3\sigma_0}{3\lambda-1}\frac{\rho_r}{3} - \frac{3}{3\lambda-1}\left[-\frac{\Lambda}{2} + \frac{\sigma_3 K^2}{18a^4} + \frac{\sigma_4 K}{6a^6}\right] + \frac{\sigma_2}{6(3\lambda-1)}\frac{K}{a^2}, \tag{10}$$

where σ_i are arbitrary constants. As in the detailed balance scenario we find $G_{\mathrm{cosmo}} = 6\sigma_0/(8\pi(3\lambda-1))$, where $\sigma_0 = \kappa^2/12$. Using the same procedure as for detailed balance in units where $8\pi G_{\mathrm{grav}} = 1$ we rewrite (9) to read:

$$H^2 = H_0^2 = \left[\frac{2}{3\lambda-1}(\Omega_{m0}(1+z)^3 + \Omega_{r0}(1+z)^4 + \omega_1 + \omega_3(1+z)^4 + \omega_4(1+z)^6] + \Omega_{k0}(1+z)^2\right], \tag{11}$$

where we have, for convenience, introduced the following dimensionless parameters, $\omega_1 = \sigma_1/(6H_0^2)$, $\omega_3 = \sigma_3 H_0^2 \Omega_{k0}^2/6$, $\omega_4 = -\sigma_4\Omega_{k0}/6$. Additionally, we impose $\omega_4 > 0$ in order for the Hubble parameter to be real for all z. Moreover, we can extract a constraint from the $z = 0$ limit of (11), which then reads $(1-\Omega_{k0})(3\lambda - 1/2 = \Omega_{m0} + \Omega_{r0} + \omega_1 + \omega_3 + \omega_4$. Much like for detailed balance, we can eliminate another parameter through constraints by considering that the ω_4 term corresponds to a quintessence-like kinetic field. Therefore it is shown in [71] and references therein that we get the following constraint at the time of BBN: $\omega_3 = 0.13424\Delta N_{\mathrm{eff}}\Omega_{r0} - \omega_4(1+z_{\mathrm{BBN}})^2$. Here $z_{\mathrm{BBN}} \approx 4\times 10^4$ is the redshift at BBN. We abbreviate the beyond detailed balance case as BDB.

III. CONSTRAINTS FROM COSMOLOGICAL DATA

A. The data

In order to carry out the parameter estimation we used a Markov-Chain Monte Carlo (MCMC) method with a large cosmological dataset. Since we are interested in the running of λ with energy, we include here a short discussion of the different energy levels of the cosmological probes we use. It is not *a priori* clear whether (or how) the running of λ depends on this energy.

Starting at high redshift (early times), our probes are the cosmic microwave background (CMB) and baryon acoustic oscillations (BAO). The CMB originates from the surface of last scattering at redshift $z_\star \sim 1100$, when the temperature of the Universe was around $T \geq 3000$ K, corresponding to an energy of around 0.26 eV. This is complemented by BAO observations, which also originate from recombination and manifest as acoustic peaks in the CMB power spectrum; however, they also affect the distribution of local galaxies and are therefore sensitive to different parameters compared to the CMB while still being an early Universe probe.

The astrophysical sources we used have different properties, in that they originate in the *late* Universe, and while the emission energies are in general higher than CMB and BAO, they do not offer any information about the state of the Universe at early times. Supernovae type 1a are used as standard rulers and outputs more energy than the rest of its host galaxy in a very short time. Their energy is less important in this context as they are used as distance rulers by fitting their spectra; however, they are certainly high-energy events, emitting neutrinos with energies up to ~40 MeV having been detected [75]. The cosmic chronometer (CC) dataset is based on passively evolving galaxies, and we only sample the expansion history with these objects. Last and most energetic, we also have gamma-ray bursts, which are the most violent explosions in the known Universe; photons from gamma-ray bursts have been found to reach energies up to 96 GeV [76]. For all details about the datasets and their implementation, see Appendix A and references therein.

B. Results

In order to derive constraints on the parameters we used (8) and its associated constraint equations in our MCMC analysis. As we are mainly interested in the running of λ we present here only the marginalized posteriors of this parameter. We include all parameter fits in Table I and II which can be found in Appendix B, where we are specifically interested in Ω_{k0} and ΔN_{eff}, since previous work ([56,67,71]) suggests that it is possible to differentiate between the two scenarios using these quantities.

In our analysis we find that in the detailed-balance scenario using all available data, λ takes the value

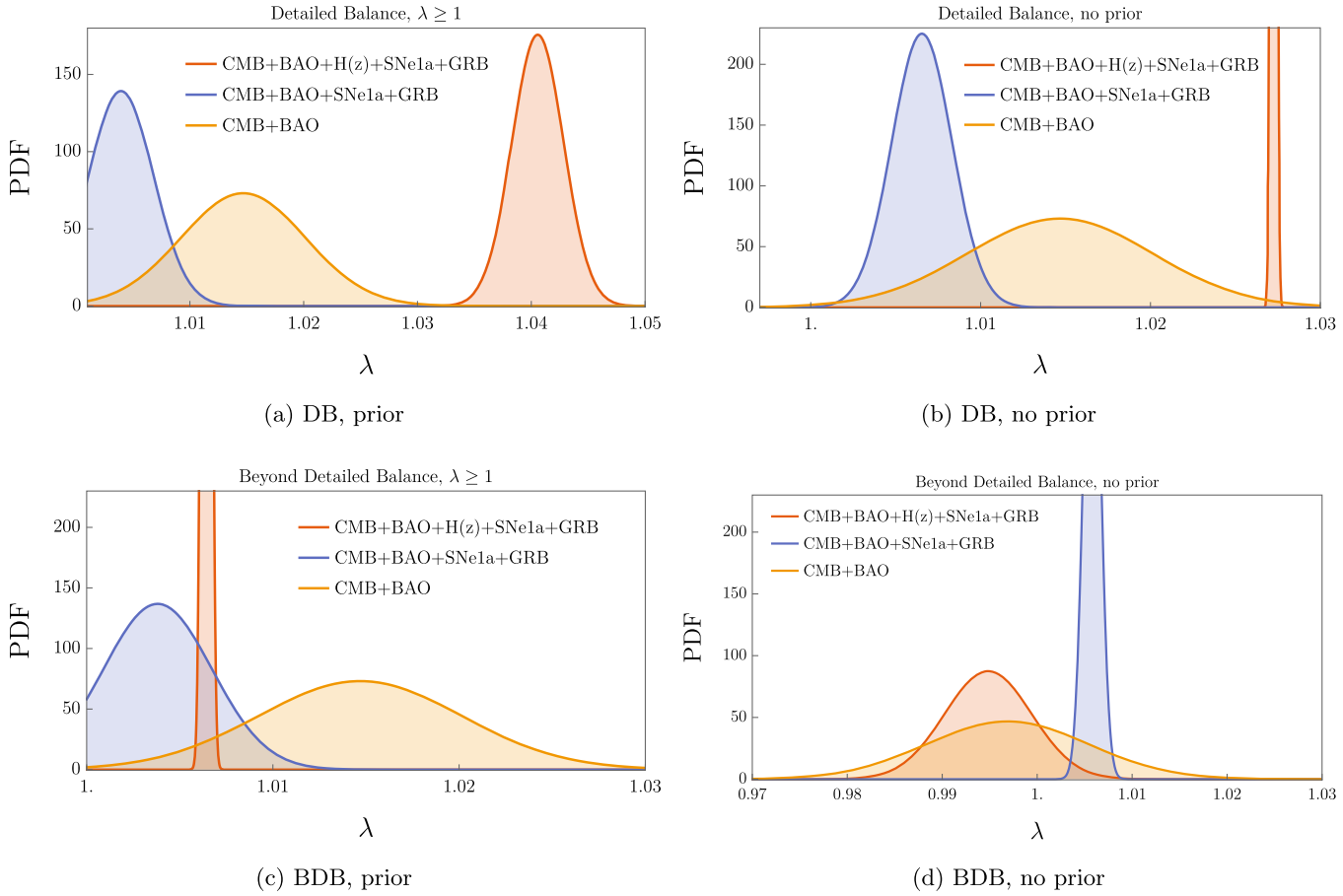

(a) DB, prior (b) DB, no prior

(c) BDB, prior (d) BDB, no prior

FIG. 1. Normalized posterior distribution functions for λ. Here, SNe1a includes Cepheid-calibrated supernovae.

$\lambda = 1.02726 \pm 0.00012$ at 1σ confidence level, when not imposing the hard prior $\lambda \geq 1$; its marginalized posterior is shown in Fig. 1(b).[4] After imposing the prior on λ, we instead obtain $\lambda = 1.046 \pm 0.0023$, and note that this value is a few percent larger, but the 1σ error bars are one order of magnitude larger, which can be seen in Fig. 1(a). In order to investigate the possible running of λ with energy, we carry out the same analysis by systematically removing data in two steps: in the first step, we remove the Hubble parameter measurements from cosmic chronometers (CC), and in the second step we remove everything except the truly early-Universe probes, CMB and BAO. For λ, the results are displayed in Fig. 1, and we observe that the results are different depending on whether we impose the detailed-balance condition or not. First of all, λ generally seems to take on higher values under detailed balance; for this case, removing CC data pushes λ to take values close to unity, but further removing data moves it back up toward higher values, but with much larger error bars. For both DB and BDB, the CMB + BAO combination seems to give the largest errors by far; this is especially pronounced in DB (no prior) and BDB (prior).

The case with the fewest assumptions and priors is the BDB (no prior) case shown in Fig. 1(c), and the situation here is somewhat reversed compared to the other three; here, removing CC data produces a higher value of λ than with the full dataset, which is in contrast to our other results. Also, the case with all data overlaps significantly with that of CMB + BAO, both of which have means firmly in the $\lambda < 1$ region. In almost all presented scenarios, in DB and BDB with the prior $\lambda \geq 1$ imposed and in DB with no prior we observe that removing Hubble data from CC strongly pushes λ close to its IR limit. Only in the BDB scenario with no imposed prior does removing that data result in λ changing sign and increasing $|\lambda - 1|$. Furthermore, removing supernovae type 1a pushes λ even further into UV, except in the BDB with no prior scenario.

Another interesting quantity to analyse is the difference between $G_{\rm grav}$ and $G_{\rm cosmo}$ which can be inferred directly from λ through the quantity $|G_{\rm cosmo}/G_{\rm grav} - 1|$. Here, we find that for detailed balance, the difference between local G and cosmological G is in general smaller than $\sim$5.8%, the largest discrepancy being in the case of all data when including a prior on λ, where we find

[4]The MCMC chains which generated the posteriors passed the standard convergence criteria detailed in [77].

$|G_{\text{cosmo}}/G_{\text{grav}} - 1| = 0.0574 \pm 0.0030$. For beyond detailed balance, this quantity takes on smaller values, generally $< 2\%$, which is of course directly linked to the values obtained on λ.

As in our previous work [67] we find here that Ω_{k0} is distinctly nonzero in the detailed balance formulation of HL cosmology, which is the same as was found in [59,60]. We also briefly point out our results on the Hubble constant, which are somewhat different from those of previous background analysis [60,67], where values close to $h = 0.71$ were found for the case of all data, which eased the Hubble parameter tension. In our present results, we find values closer to that of ΛCDM, with $h = 0.6488 \pm 0.0012$ for DB and $h = 0.6813 \pm 0.048$ for BDB, both with all data; the BDB value closely resembles that obtained by *Planck* ($h = 0.6844 \pm 0.091$) using TE + lowE spectra while assuming a base ΛCDM model. On the other hand, the DB case takes values close to the *Planck* TT + TE + EE + lowE + lensing results when considering a ΛCDM model extended by allowing for a nonzero ΔN_{eff} [78]. A full analysis of the Hubble tension lies beyond the scope of this paper.

Another interesting result is the value of ΔN_{eff}, which takes on values greater than 0.2 in almost all cases, and a 1σ upper limit of $\Delta N_{\text{eff}} \leq 0.75$ for BDB (prior, all data). As this is slightly surprising it is worth reiterating that this chain passed all convergence criteria detailed in [77]. Therefore, with all other parameters taking on reasonable values (and similar results found in [60,67]) one may have to entertain the possibility of a fourth neutrino species present in HL cosmology. Indeed, it was recently suggested that a fourth neutrino might solve the H_0 tension problem [79]; in this paper, the authors arrive at a value of $N_{\text{eff}} \approx 4$ (effective number of neutrino species), which is far higher than our results. Moreover, our results fall outside BBN limits as reported in [80,81] ($-1.7 \leq \Delta N_{\text{eff}} \leq 2.0$), but seem to agree somewhat with limits from CMB ($\Delta N_{\text{eff}} < 0.2$) [82]. The fact that $\Delta N_{\text{eff}} \neq 0$ in both scenarios fits with the nonflatness results indicated by Ω_{k0}. In fact, a closed Universe Ω_{k0} has been found in several different analyses of Hořava-Lifshitz cosmology [59,60,67], and it now seems that the model does indeed prefer a closed Universe. Other studies have reported a strong preference for a closed Universe in the *Planck* data [83], a result which is sensitive to the amount of lensing in the sample. Other datasets, primarily BAO, strongly favor a closed Universe (under the assumption of ΛCDM) to the extent that the tension in Ω_{k0} has been estimated at $2.5 - 3\sigma$ [62].

IV. DISCUSSION AND CONCLUSIONS

The focus of this paper is exploring the significance of the parameter λ in HL cosmology, which is believed to play a crucial role in determining or characterizing the extent of Lorentz violation present in the theory. Our primary objective was to examine the impact of incorporating or omitting data sources corresponding to different energy levels on the estimated value of λ. In other words, we wanted to investigate whether there is a correlation between the energy level and the value of λ.

In the detailed-balance scenario, our findings indicate that the parameter λ consistently exceeds unity at a 1σ level; however, if we exclude low-energy sources, such as Hubble parameter measurements, the value of λ tends to shift closer to the ultraviolet region. In the case of beyond detailed balance, we observed a mean value below unity in two instances. While the relationship between energy flow and λ is not as evident here as in the detailed-balance scenario, we can still observe a clear trend: when the lowest-energy data is removed, λ is pushed below unity. The trend observed in the behavior of λ when excluding low-energy sources is more important than its specific values and seems to be consistent with the underlying theory. We have also performed the same calculations when considering the hard prior $\lambda \geq 1$, since the parameter range $1/3 < \lambda < 1$ results in nonunitary quantum evolution and therefore is generally avoided in the theoretical considerations. Nonetheless, we present general results both with and without that prior on λ in order to have a more complete picture of the theory. In the case when the prior $\lambda \geq 1$ is imposed, excluding low energy data changes the BDB case more, since this model has a stronger tendency to flow to $\lambda < 1$ without a prior, but also the DB case sees changes, especially on the form of larger errors on the case with all data, although the reason for this is not clear. The key takeaway point of this paper is that we observe statistically different bounds on λ depending on the probe used, and in the DB case, λ is consistently larger than unity when no prior on λ is imposed. Although this may be an artefact of picking datasets, the results imply that taking the running of λ into account may be necessary even in relatively low-energy regime. We expect this effect to become pronounced in truly UV environments such as the early Universe.

The phenomenological results obtained suggest the potential existence of Lorentz violation in astrophysical probes at higher energies; however, it is important to note that the existing bounds on Lorentz violation in the matter and electromagnetic sectors are significantly stronger than those in the gravity sector [84–86]. Several theoretical studies have been dedicated to addressing this issue [87–90], proposing additional terms to the action aimed at preventing the leakage of symmetry violations from the gravity sector to the matter sector or suppressing them in the low-energy regime of the matter sector. Recent results of [51] on Einstein aether/ khronometric theories, with the IR limit of non-projectable Hořava gravity being equivalent to the khronometric theory, [63] actually seem to favor the preferred frame/ foliation theories over GR, or at least fitting observational data just as well. Obtained constrains on PPN parameters describing preferred-frame effects, although very tightly constrained, seem to have probability distributions at 1σ bounded away from zero, its GR value.

A natural question which also arises is how the parameter λ would vary in different nonprojectable extensions of HL gravity, which have been proposed to address some of its shortcomings. While work on these scenarios is ongoing, it is important to note that relaxing projectability conditions leads to a more complex theory with a higher number of parameters and interpretation issues. For now, we present our current findings, which are intriguing and merit further theoretical and observational investigation. These results could offer new insights into the underlying HL theory.

ACKNOWLEDGMENTS

This work has been cofinanced by Military University of Technology (ECz) under research Project No. UGB 703/WAT/2024. NAN was financed by CNES and IBS under the project code IBS-R018-D3, and acknowledges support from PSL/Observatoire de Paris, as well as for discussions with Vincenzo Salzano.

APPENDIX A: THE DATA

1. *Planck* CMB

The nonperturbative CMB information is contained in the shift parameters, describing the location of the first peak in the temperature angular power spectrum. Here, we use the shift parameters extracted from the final *Planck* 2018 data release [78]. For a vector $\boldsymbol{\theta}$ containing the model parameters, the geometrical CMB shift parameters read

$$R(\boldsymbol{\theta}) = 100\sqrt{\Omega_{m0}h^2}\frac{d_A^c(z_*,\boldsymbol{\theta})}{c}, \qquad \ell_a(\boldsymbol{\theta}) = \pi\frac{d_A^c(z_*,\boldsymbol{\theta})}{r_s(z_*,\boldsymbol{\theta})}, \tag{A1}$$

which together with $\omega_b = \Omega_{b0}h^2$ makes up the CMB distance priors. In the above equations, $d_A^c(z_*,\boldsymbol{\theta})$ and $r_s(z_*,\boldsymbol{\theta})$ are the comoving angular-diameter distance and the sound horizon, respectively, defined as

$$d_A^c(z,\boldsymbol{\theta}) = \begin{cases} \frac{c}{H_0}\frac{1}{\sqrt{\Omega_{k0}}}\sinh\left[\sqrt{\Omega_{k0}}\int_0^z\frac{dz'}{E(z',\boldsymbol{\theta})}\right], & \Omega_{k0}>0 \\ \frac{c}{H_0}\int_0^z\frac{dz'}{E(z',\boldsymbol{\theta})}, & \Omega_{k0}=0 \\ \frac{c}{H_0}\frac{1}{\sqrt{|\Omega_{k0}|}}\sinh\left[\sqrt{|\Omega_{k0}|}\int_0^z\frac{dz'}{E(z',\boldsymbol{\theta})}\right], & \Omega_{k0}>0, \end{cases} \tag{A2}$$

and

$$r_s(z,\boldsymbol{\theta}) = H_0\int_z^\infty\frac{c_s(z')dz'}{E(z',\boldsymbol{\theta})}, \tag{A3}$$

where $E(z,\boldsymbol{\theta}) \equiv H(z,\boldsymbol{\theta})/H_0$ and $c_s(z)$ is the sound speed

$$c_s(z) = \frac{c}{\sqrt{3[1+R_b/(1+z)]}}, \qquad R_b = 31500\omega_b\left(\frac{T_{\rm CMB}}{2.72}\right)^{-4}. \tag{A4}$$

The above relations are defined at the photon-decoupling redshift z_*, which is defined as [91]

$$\begin{aligned} z_* &= 1048[1+0.00124\omega_b^{-0.738}][1+g_1\omega_b^{g_2}] \\ g_1 &= 0.0783\omega_b^{-0.238}[1+39.5\omega_b^{-0.763}]^{-1} \\ g_2 &= 0.560[1+21.1\omega_b^{1.81}]^{-1}. \end{aligned} \tag{A5}$$

In the model we are considering, the number of relativistic species are no longer equal to the ΛCDM value of $N_{\rm eff} = 3.046$, and since the value of this quantity have several effects on the CMB, we need now to incorporate this into the analysis. Following the procedure in [92], we add the CDM density parameter $\omega_c = (\Omega_{m0} - \Omega_{b0})h^2$ and $N_{\rm eff} = 3.046 + \Delta N_{\rm eff}$, and the full CMB distance priors read $\boldsymbol{v} = (R, \ell_a, \omega_b, \omega_c, N_{\rm eff})$. We use the values found in [92]

$$\boldsymbol{v} = \begin{pmatrix} 1.7661 \\ 301.7293 \\ 0.02191 \\ 0.1194 \\ 2.8979, \end{pmatrix} \tag{A6}$$

as well as the associated covariance matrix

$$C_{\boldsymbol{v}} = 10^{-8}\begin{pmatrix} 33483.54 & -44417.15 & -515.03 & -360.42 & -274151.72 \\ -44417.15 & 4245661.67 & 2319.46 & 63326.47 & 4287810.44 \\ -515.03 & 2319.46 & 12.92 & 51.98 & 7273.04 \\ -360.42 & 63326.47 & 51.98 & 1516.28 & 92013.95 \\ -274151.72 & 4287810.44 & 7273.04 & 92013.95 & 7876074.60 \end{pmatrix} \tag{A7}$$

and the CMB χ^2 finally reads

$$\chi^2_{\rm CMB} = (\Delta \boldsymbol{\nu})\ {}^{\rm T}C_{\boldsymbol{\nu}}^{-1}\Delta\boldsymbol{\nu}, \tag{A8}$$

where $\Delta\boldsymbol{\nu}$ is the difference between the theoretical and observed values of the distance priors $\boldsymbol{\nu}$.

2. Pantheon + and Cepheid variable stars

The Pantheon + sample is a set of 1701 light curves of 1550 distinct supernovae type Ia (SNeIa) in the redshift range $0.001 < z < 2.26$ [93,94]. Compared to the previous catalog Pantheon, this update features an increased redshift range of cross-calibrated photometric systems of sources and improved treatment of systematic effects; all together, this results in an factor of 2 improvement in cosmological constraining power [94]. Also contained in this catalog are those SNeIa from host galaxies with known Cepheid distances, providing a robust calibration of the SNeIa light curve (known as "anchoring") and enables the simultaneous determination of expansion-history parameters (for example Ω_{m0}) and the local expansion rate H_0, which are degenerate when using SNeIa alone.

In order to form the χ^2 for Pantheon, we write down the luminosity distance as (all details can be found in [94])

$$d_L(z,\boldsymbol{\theta}) = (1+z_{\rm hel})d_A^c(z,\boldsymbol{\theta}), \tag{A9}$$

where $z_{\rm hel}$ is the redshift measured in the heliocentric frame. From this we can define distance modulus as

$$\mu(z,\boldsymbol{\theta}) = m(z,\boldsymbol{\theta}) - M, \tag{A10}$$

where m and M is the apparent and fiducial absolute magnitude, respectively. From this expression, we can write the apparent magnitude as

$$m(z,\boldsymbol{\theta}) = 5\log d_L(z,\boldsymbol{\theta}) + 25 + M, \tag{A11}$$

where $d_L(z,\boldsymbol{\theta})$ is now expressed in Mpc. Note here that we are not able to simply write the distance modulus as $\mu = m - M = 5\log d_L + \mu_0$ and marginalize over μ_0; when using SNeIa alone, M can indeed be marginalized over, but including Cepheids breaks the degeneracy between M and H_0, and the fiducial absolute magnitude M becomes an extra free parameter in our numerical analysis. As such, we write the distance residuals as [94]

$$\Delta D_i = \begin{cases} \mu_i - \mu_i^C, & i \in \text{Cepheids} \\ \mu_i - \mu_i^{\rm model} & \text{others}, \end{cases} \tag{A12}$$

where the theoretical value is replaced by the corresponding Cepheid-calibrated value for the host galaxy distance, hence providing the anchoring and breaking the degeneracy between Ω_{m0} and M. The statistical and systematic uncertainties are contained in the covariance matrix $C_{\rm stat+sys}^{\rm SN+Cepheids}$, and the χ^2 measure becomes

$$\chi^2_{\rm Pantheon+Cepheids} = (\Delta\boldsymbol{D})^{\rm T}\left(C_{\rm stat+sys}^{\rm SN+Cepheids}\right)^{-1}(\Delta\boldsymbol{D}) \tag{A13}$$

3. Gamma-ray bursts

Gamma-ray bursts are one of the most energetic events in the Universe, and may be used as a probe complementing SNeIa [95]. This sample consists of 79 long gamma-ray bursts (the Mayflower sample) calibrated using the Padé approximant method. This approach avoids the circularity problem usually present when trying to use gamma-ray bursts as cosmological rulers [96]. The χ^2 for this dataset is found by considering the distance modulus (as for SNeIa, but we can now marginalize over μ_0), and we write the χ^2 as

$$\chi^2_{\rm GRB} = a + \log\frac{e}{2\pi} - \frac{b^2}{e}, \tag{A14}$$

where $a = (\Delta\mu)^{\rm T}C_{\rm GRB}^{-1}(\Delta\mu)$, $b = (\Delta\mu)^{\rm T}C_{\rm GRB}^{-1}\cdot\mathbf{1}$, and $c = \mathbf{1}^{\rm T}\cdot C_{\rm GRB}^{-1}\cdot\mathbf{1}$. Here we have defined $\Delta\mu = \mu_{\rm theory} - \mu_{\rm obs}$ where $\mu_{\rm obs}$ is the observed distance modulus, and $\mu_{\rm theory}$ comes from the Padé method after calibration. The full details of this calibration and the data can be found in [95].

4. Cosmic chronometers (CC)

We use Hubble-parameter measurements from passively-evolving early-type galaxies (ETG), which have low star-formation rate and old stellar populations. The spectral properties of ETGs can be traced along cosmic time t by measuring the Hubble parameter $H(z) = dz/dt(1+z)$ independent of the cosmological model [97], making them a type of standardisable clock, or cosmic chronometer. We use a sample covering the redshift range $0 < z < 1.97$ [98–100]. To construct a covariance matrix for the CC data points we follow the procedure in [101,102], which includes the following sources of uncertainty

$$C_{\rm CC} = C_{\rm CC}^{\rm stat} + C_{\rm CC}^{\rm young} + C_{\rm CC}^{\rm model} + C_{\rm CC}^{\rm met}, \tag{A15}$$

where $C_{\rm CC}^{\rm stat}$, $C_{\rm CC}^{\rm young}$, and $C_{\rm CC}^{\rm model}$ correspond to uncertainty from statistical errors, sample-contamination by younger (and hotter) stars, model dependence, and stellar metallicity. In these considerations, the largest source of error comes from the $C_{\rm CC}^{\rm young}$ contribution [102]. The model uncertainty $C_{\rm CC}^{\rm model}$ can be further broken down into

$$C_{\rm CC}^{\rm model} = C_{\rm CC}^{\rm SFH} + C_{\rm CC}^{\rm IMF} + C_{\rm CC}^{\rm stlib} + C_{\rm CC}^{\rm SPS}, \tag{A16}$$

denoting star-formation history (SFH), initial mass function (IMF), stellar library (st.lib.), and stellar population synthesis (SPS). We use the accompanying code[5] [102] to generate the final covariance matrix for our data points, after which the χ^2 reads

$$\chi^2_{\rm CC} = (\Delta H)^{\rm T} C^{-1}_{\rm CC} (\Delta H), \tag{A17}$$

where $(\Delta H)_i = H_{\rm theory}(z_i) - H_{\rm obs}(z_i)$.

5. Baryon acoustic oscillations

We include seven different BAO datasets in our analysis, as shown below

WiggleZ: We include data from the WiggleZ Dark Energy Survey at redshift points $z_W = \{0.44, 0.6, 0.73\}$ [103]. Here, the observables are

$$A(x,\boldsymbol{\theta}) = 100\sqrt{\omega_m}\frac{D_V(z,\boldsymbol{\theta})}{cz}, \qquad F(z,\boldsymbol{\theta}) = \frac{d^c_A(z,\boldsymbol{\theta})H(z,\boldsymbol{\theta})}{c}, \tag{A18}$$

where $A(x,\boldsymbol{\theta})$ is the acoustic parameter, $F(z,\boldsymbol{\theta})$ is the Alcock-Paczynski distortion parameter, and $\omega_m = \Omega_{m0}h^2$. $D_V(z,\boldsymbol{\theta})$ is the volume distance, defined as

$$D_V(z,\boldsymbol{\theta}) = \left[d^c_A(z,\boldsymbol{\theta})^2 \frac{cz}{H(z,\boldsymbol{\theta})}\right]^{1/3}, \tag{A19}$$

and we find the χ^2 as

$$\chi^2_W = (\Delta\mathcal{F}_W)^{\rm T} C^{-1}_W \Delta\mathcal{F}_W, \tag{A20}$$

where $\Delta\mathcal{F}_W = \mathcal{F}_{W,\rm theory} - \mathcal{F}_{W,\rm obs}$, and $\mathcal{F}_W = \{A(z_W), F(z_W)\}$. For all the other BAO probes, we find the χ^2 in the same way.

SDSS-BOSS: we include data from the SDSS-II BOSS DR12 and SDSS-IV DR16 LRG (Luminous Red Galaxy growth-rate sample) at redshifts $z_{\rm B} = \{0.38, 0.51, 0.61\}$. For this data, we use the quantities

$$d^c_A(z,\boldsymbol{\theta})\frac{r^{\rm fid}_s(z_d)}{r_s(z_d,\boldsymbol{\theta})}, \qquad H(z,\boldsymbol{\theta})\frac{r_s(z_d,\boldsymbol{\theta})}{r^{\rm fid}_s(z_d)}, \tag{A21}$$

evaluated at the dragging redshift z_d, which we approximate as [104]

$$\begin{aligned} z_d &= 1291\frac{\omega_m^{0.251}}{1+0.659\omega_m^{0.828}}(1+b_1\omega_b{}^{b_2}) \\ b_1 &= 0.313\omega_m^{-0.419}(1+0.607\omega_m^{0.6748}) \\ b_2 &= 0.238\omega_m^{0.223}. \end{aligned} \tag{A22}$$

In Eq. (A21) $r^{\rm fid}_s$ is the sound horizon at the dragging redshift evaluated for a fiducial cosmological model; here, we take $r^{\rm fid}_s(z_d) = 147.78$ Mpc [105,106].

SDSS QSO: From the SDSS IV BOSS DR14 quasar sample, we have the following data points at redshifts $z_Q = \{0.978, 1.23, 1.526, 1.944\}$ [107]

$$\begin{aligned} d^c_A\frac{r^{\rm fid}_s(z_d)}{r_s(z_d} &= \{1586.18 \pm 284.93, 1769.08 \pm 159.67, 1768.77 \pm 96.59, 1807.98 \pm 146.46\} \\ H\frac{r_s(z_d)}{r^{\rm fid}_s(z_d)} &= \{113.72 \pm 14.63, 131.44 \pm 12.42, 148.11 \pm 12.75, 172.63 \pm 14.79\} \\ D_V\frac{r^{\rm fid}_s(z_d)}{r_s(z_d)} &= \{2933.59 \pm 327.71, 3522.04 \pm 192.74, 3954.31 \pm 141.71, 4575.17 \pm 241.61\}. \end{aligned} \tag{A23}$$

From the eBOSS DR16 QSO release [108,109], we also have the following data points at redshift $z = 1.480$

$$\frac{c}{Hr_s(z_d)} = 13.23 \pm 0.47, \qquad \frac{d^c_A}{r_s(z_d)} = 30.21 \pm 0.79. \tag{A24}$$

eBOSS ELG: from the eBOSS DR16 Emission Line Galaxy sample (ELG) we have, at the effective redshift $z_{\rm eff} = 0.845$ [110,111]

$$\frac{c}{Hr_s(z_{\rm eff})} = 19.6^{+2.2}_{-2.1}, \qquad \frac{d^c_A(z_{\rm eff})}{r_s(z_d)} = 19.5 \pm 1 \tag{A25}$$

eBOSS CMASS: from void-galaxy cross-correlations in redshift-space distortion corrected data from the DR12 LRG CMASS sample, we have, at the effective sample redshift of $z_{\rm eff} = 0.69$ the following [112]

$$\frac{c}{Hr_s(z_{\rm eff})} = 17.48 \pm 0.23, \qquad \frac{d^c_A(z_{\rm eff})}{r_s(z_d)} = 20.10 \pm 0.34. \tag{A26}$$

Lyman-α: using the autocorrelation of Lyman-α absorption in quasars and Lyman-α cross correlation in the eBOSS DR16 quasar sample [113] we have (at the effective redshift $z_{\rm eff} = 2.33$)

$$\frac{c}{Hr_s(z_{\rm eff})} = 8.99 \pm 0.19, \qquad \frac{d^c_A(z_{\rm eff})}{r_s(z_d)} = 37.5 \pm 1.1. \tag{A27}$$

All the χ^2 measures for the above BAO points are included in our analysis.

[5] https://gitlab.com/mmoresco/CCcovariance.

APPENDIX B: ALL PARAMETER CONSTRAINTS

TABLE I. Parameter constraints at 1σ for the detailed balance case, with and without a hard prior on the parameter λ. † implies a one-sided upper bound resulting from a hard uniform prior, and bold indicates a particularly noisy parameter.

	Detailed balance, prior $\lambda \geq 1$			Detailed balance, no prior on λ		
Parameter	CMB + BAO + H(z) + SNe1a + Cepheids + GRB	CMB + BAO + SNe1a + Cepheids + GRB	CMB + BAO	CMB + BAO + H(z) + SNe1a + Cepheids + GRB	CMB + BAO + SNe1a + Cepheids + GRB	CMB + BAO
Ω_b	0.0049768 ± 0.0000016	$0.04898^{+0.00055}_{-0.000053}$	0.05104 ± 0.00080	0.049236 ± 0.000070	0.04907 ± 0.00058	$0.05139^{+0.00019}_{-0.00020}$
$\Omega_b h^2$	0.020952 ± 0.000074	0.02227 ± 0.00018	$0.02192^{+0.00019}_{-0.00021}$	0.02158 ± 0.00012	0.02217 ± 0.00017	0.02187 ± 0.00011
Ω_m	0.3336 ± 0.0018	$0.3153^{+0.0057}_{-0.0055}$	0.3398 ± 0.0083	0.3204 ± 0.0030	0.3170 ± 0.0056	$0.34437^{+0.00010}_{-0.00012}$
$\Omega_m h^2$	$0.14043^{+0.00024}_{-0.00025}$	0.14335 ± 0.00090	$0.1458^{+0.0011}_{-0.0010}$	$0.14047^{+0.00030}_{-0.00033}$	0.14323 ± 0.00092	0.14657 ± 0.00023
$\Omega_k 10^4$	-4.1364 ± 0.0040	$-6.116^{+1.55}_{-0.30}$	$-11.60^{+2.61}_{-1.76}$	-4.254 ± 0.019	-5.745 ± 0.029	$-13.5030^{+0.0088}_{-0.0086}$
$\Omega_r 10^5$	$9.937^{+0.036}_{-0.035}$	9.20 ± 0.12	$9.74^{+0.19}_{-0.18}$	$9.543^{+0.070}_{-0.065}$	$9.259^{+0.012}_{-0.011}$	$9.83^{+0.012}_{-0.018}$
h	0.6488 ± 0.0012	$0.6743^{+0.0043}_{-0.0044}$	$0.6553^{+0.0061}_{-0.0063}$	$0.6621^{+0.0023}_{-0.0024}$	0.6722 ± 0.0040	0.65239 ± 0.00040
M	-19.5051 ± 0.0013	$-19.437^{+0.012}_{-0.013}$	...	-19.4783 ± 0.0075	-19.442 ± 0.012	...
$\Delta N_{\rm eff}$	0.0046750 ± 0.0000076	$\mathbf{0.1104^{+0.0011}_{-0.0049}}$	$0.038^{+0.013}_{-0.015}$	0.005099 ± 0.000060	0.009670 ± 0.000062	0.05195 ± 0.00019
λ	1.0406 ± 0.0023	$< \mathbf{1.0032}^{\dagger}$	$1.0146^{+0.055}_{-0.053}$	1.02726 ± 0.00012	1.0065 ± 0.0018	1.0159 ± 0.0014
$\lvert\frac{G_{\rm cosmo}}{G_{\rm grav}} - 1\rvert$	0.0574 ± 0.0030	$< \mathbf{0.0035}^{\dagger}$	$0.0214^{+0.0078}_{-0.0077}$	0.03928 ± 0.00017	$0.00997^{+0.0026}_{-0.0025}$	0.0232 ± 0.0020
$\chi^2_{\rm min}$	1778.27	1635.41	27.30	1705.04	1638.49	27.76

TABLE II. Parameter constraints at 1σ for the Beyond Detailed Balance case, with and without a hard prior on the parameter λ. † implies a one-sided upper bound resulting from a hard uniform prior.

	Beyond detailed balance, prior $\lambda \geq 1$			Beyond detailed balance, no prior on λ		
Parameter	CMB + BAO + H(z) + SNe1a + Cepheids + GRB	CMB + BAO + SNe1a + Cepheids + GRB	CMB + BAO	CMB + BAO + H(z) + SNe1a + Cepheids + GRB	CMB + BAO + SNe1a + Cepheids + GRB	CMB + BAO
Ω_b	$0.049371^{+0.00049}_{-0.00048}$	0.05024 ± 0.00049	$0.05116^{+0.00062}_{-0.00063}$	0.04900 ± 0.00040	$0.05034^{+0.00017}_{-0.00016}$	0.05034 ± 0.00016
$\Omega_b h^2$	0.022922 ± 0.00023	0.02262 ± 0.00020	0.02226 ± 0.00018	0.022864 ± 0.00011	0.02250 ± 0.00011	0.02250 ± 0.00011
Ω_m	0.3198 ± 0.0053	$0.3194^{+0.0056}_{-0.0054}$	0.3349 ± 0.0073	$0.3109^{+0.0038}_{-0.0041}$	0.3232 ± 0.0031	$0.3284^{+0.0093}_{-0.0091}$
$\Omega_m h^2$	0.1484 ± 0.0017	$0.14386^{+0.00095}_{-0.00096}$	0.1458 ± 0.0011	$0.14509^{+0.00015}_{-0.00016}$	$0.14442^{+0.00046}_{-0.00049}$	$0.1458^{+0.0030}_{-0.0027}$
$\Omega_k 10^3$	$-9.71^{+1.73}_{-1.83}$	$-4.98^{+0.77}_{-0.46}$	-3.93 ± 0.15	$-5.399^{+0.022}_{-0.023}$	-4.338 ± 0.080	-6.32 ± 2.56
$\Omega_r 10^5$	9.01 ± 0.13	9.29 ± 0.11	$9.61^{+1.63}_{-1.61}$	$8.97^{+1.06}_{-1.11}$	9.36 ± 0.61	$9.431^{+0.028}_{-0.030}$
h	0.6813 ± 0.0048	$0.6711^{+0.0039}_{-0.0040}$	$0.6599^{+0.0056}_{-0.0055}$	$0.6831^{+0.0043}_{-0.0040}$	$0.6685^{+0.0022}_{-0.0021}$	$0.6660^{+0.0109}_{-0.0096}$
M	$-19.414^{+0.014}_{-0.015}$	-19.446 ± 0.0011	...	$-19.412^{+0.012}_{-0.011}$	-19.4525 ± 0.0040	...
$\Delta N_{\rm eff}$	0.61 ± 0.14	$0.258^{+0.028}_{-0.048}$	0.198 ± 0.015	$0.2578^{+0.0042}_{-0.0044}$	0.2166 ± 0.0070	$0.31^{+0.19}_{-0.15}$
λ	1.00644 ± 0.00020	$< 1.0068^{\dagger}$	1.0065 ± 0.0025	$0.9949^{+0.0045}_{-0.0046}$	1.00578 ± 0.00086	$0.9972^{+0.0081}_{-0.0088}$
$\lvert\frac{G_{\rm cosmo}}{G_{\rm grav}} - 1\rvert$	0.00957 ± 0.00029	$< 0.010^{\dagger}$	0.0096 ± 0.0037	$0.0078^{+0.0070}_{-0.0053}$	0.0086 ± 0.0013	< 0.019
ω_1	0.69957 ± 0.00039	$0.6909^{+0.0063}_{-0.0062}$	$0.6789^{+0.0070}_{-0.0075}$	0.6866 ± 0.0036	$0.6898^{+0.0044}_{-0.0043}$	0.6898 ± 0.0043
$\omega_3 10^6$	$7.07^{+1.62}_{-1.71}$	$1.77^{+0.10}_{-0.15}$	$1.5201^{+0.068}_{-0.071}$	$2.9109^{+0.047}_{-0.0049}$	1.80 ± 0.15	1.79 ± 0.15
$\chi^2_{\rm min}$	1634.37	1632.36	23.82	1635.54	1633.85	21.85

[1] P. Horava, Spectral dimension of the universe in quantum gravity at a Lifshitz point, Phys. Rev. Lett. **102**, 161301 (2009).

[2] R. Bluhm, Explicit versus spontaneous diffeomorphism breaking in gravity, Phys. Rev. D **91**, 065034 (2015).

[3] R. L. Arnowitt, S. Deser, and C. W. Misner, The dynamics of general relativity, Gen. Relativ. Gravit. **40**, 1997 (2008).

[4] T. P. Sotiriou, M. Visser, and S. Weinfurtner, Quantum gravity without Lorentz invariance, J. High Energy Phys. 10 (2009) 033.

[5] C. Bogdanos and E. N. Saridakis, Perturbative instabilities in Horava gravity, Classical Quantum Gravity **27**, 075005 (2010).

[6] K. Koyama and F. Arroja, Pathological behaviour of the scalar graviton in Hořava-Lifshitz gravity, J. High Energy Phys. 03 (2010) 061.

[7] D. Blas, O. Pujolas, and S. Sibiryakov, On the extra mode and inconsistency of Hořava gravity, J. High Energy Phys. 10 (2009) 029.

[8] D. Blas, O. Pujolas, and S. Sibiryakov, Models of non-relativistic quantum gravity: The Good, the bad and the healthy, J. High Energy Phys. 04 (2011) 018.

[9] D. Blas, O. Pujolas, and S. Sibiryakov, Consistent extension of Hořava gravity, Phys. Rev. Lett. **104**, 181302 (2010).

[10] T. P. Sotiriou, Hořava-Lifshitz gravity: A status report, J. Phys. Conf. Ser. **283**, 012034 (2011).

[11] D. Vernieri and T. P. Sotiriou, Hořava-Lifshitz gravity: Detailed balance revisited, Phys. Rev. D **85**, 064003 (2012).

[12] C. Appignani, R. Casadio, and S. Shankaranarayanan, The cosmological constant and Horava-Lifshitz gravity, J. Cosmol. Astropart. Phys. 04 (2010) 006.

[13] C. Charmousis, G. Niz, A. Padilla, and P. M. Saffin, Strong coupling in Hořava gravity, J. High Energy Phys. 08 (2009) 070.

[14] D. Vernieri, On power-counting renormalizability of Hořava gravity with detailed balance, Phys. Rev. D **91**, 124029 (2015).

[15] M. Colombo, A. E. Gümrükçüoğlu, and T. P. Sotiriou, Hořava gravity with mixed derivative terms: Power counting renormalizability with lower order dispersions, Phys. Rev. D **92**, 064037 (2015).

[16] S. Mukohyama, Horava-Lifshitz cosmology: A review, Classical Quantum Gravity **27**, 223101 (2010).

[17] K. Izumi and S. Mukohyama, Nonlinear superhorizon perturbations in Horava-Lifshitz gravity, Phys. Rev. D **84**, 064025 (2011).

[18] A. E. Gumrukcuoglu, S. Mukohyama, and A. Wang, General relativity limit of Horava-Lifshitz gravity with a scalar field in gradient expansion, Phys. Rev. D **85**, 064042 (2012).

[19] B. Audren, D. Blas, M. M. Ivanov, J. Lesgourgues, and S. Sibiryakov, Cosmological constraints on deviations from Lorentz invariance in gravity and dark matter, J. Cosmol. Astropart. Phys. 03 (2015) 016.

[20] F. G. Alvarenga, L. A. M. Diniz, S. V. B. Gonçalves, G. A. Monerat, and E. V. Corrêa Silva, Observational constraints on the quantum Einstein-Aether model, Eur. Phys. J. Plus **138**, 975 (2023).

[21] A. O. Barvinsky, D. Blas, M. Herrero-Valea, S. M. Sibiryakov, and C. F. Steinwachs, Renormalization of Hořava gravity, Phys. Rev. D **93**, 064022 (2016).

[22] A. O. Barvinsky, M. Herrero-Valea, and S. M. Sibiryakov, Towards the renormalization group flow of Horava gravity in $(3+1)$ dimensions, Phys. Rev. D **100**, 026012 (2019).

[23] A. O. Barvinsky, D. Blas, M. Herrero-Valea, S. M. Sibiryakov, and C. F. Steinwachs, Hořava gravity is asymptotically free in $2+1$ dimensions, Phys. Rev. Lett. **119**, 211301 (2017).

[24] A. O. Barvinsky, A. V. Kurov, and S. M. Sibiryakov, Beta functions of $(3+1)$-dimensional projectable hořava gravity, Phys. Rev. D **105**, 044009 (2022).

[25] D. Blas, Hořava gravity: Motivation and status, J. Phys. Conf. Ser. **952**, 012002 (2018).

[26] J. Bellorin, C. Borquez, and B. Droguett, Cancellation of divergences in the nonprojectable Hořava theory, Phys. Rev. D **106**, 044055 (2022).

[27] S. Mukohyama, Dark matter as integration constant in Horava-Lifshitz gravity, Phys. Rev. D **80**, 064005 (2009).

[28] S. Mukohyama, Caustic avoidance in Horava-Lifshitz gravity, J. Cosmol. Astropart. Phys. 09 (2009) 005.

[29] S. Mukohyama, Scale-invariant cosmological perturbations from Horava-Lifshitz gravity without inflation, J. Cosmol. Astropart. Phys. 06 (2009) 001.

[30] S. F. Bramberger, A. Coates, J. a. Magueijo, S. Mukohyama, R. Namba, and Y. Watanabe, Solving the flatness problem with an anisotropic instanton in Hořava-Lifshitz gravity, Phys. Rev. D **97**, 043512 (2018).

[31] H. Matsui and S. Mukohyama, Hartle-Hawking no-boundary proposal and Hořava-Lifshitz gravity, Phys. Rev. D **109**, 023504 (2024).

[32] B. Cropp, S. Liberati, A. Mohd, and M. Visser, Ray tracing Einstein-Æther black holes: Universal versus Killing horizons, Phys. Rev. D **89**, 064061 (2014).

[33] J. Bhattacharyya, M. Colombo, and T. P. Sotiriou, Causality and black holes in spacetimes with a preferred foliation, Classical Quantum Gravity **33**, 235003 (2016).

[34] F. Michel and R. Parentani, Black hole radiation in the presence of a universal horizon, Phys. Rev. D **91**, 124049 (2015).

[35] M. Herrero-Valea, S. Liberati, and R. Santos-Garcia, Hawking radiation from universal horizons, J. High Energy Phys. 04 (2021) 255.

[36] N. Oshita, N. Afshordi, and S. Mukohyama, Lifshitz scaling, ringing black holes, and superradiance, J. Cosmol. Astropart. Phys. 05 (2021) 005.

[37] G. Lara, M. Herrero-Valea, E. Barausse, and S. M. Sibiryakov, Black holes in ultraviolet-complete Hořava gravity, Phys. Rev. D **103**, 104007 (2021).

[38] G.-P. Li and K.-J. He, Shadows and rings of the Kehagias-Sfetsos black hole surrounded by thin disk accretion, J. Cosmol. Astropart. Phys. 06 (2021) 037.

[39] K. Jusufi, H. Hassanabadi, P. Sedaghatnia, J. Kríz, W. S. Chung, H. Chen, Z.-L. Zhao, and Z. W. Long, Thermodynamics and shadow images of charged black holes in Horava-Lifshitz gravity, Eur. Phys. J. Plus **137**, 1147 (2022).

[40] O. Bertolami and C. A. D. Zarro, Hořava-Lifshitz quantum cosmology, Phys. Rev. D **84**, 044042 (2011).

[41] T. Christodoulakis and N. Dimakis, Classical and quantum Bianchi Type III vacuum Horava-Lifshitz cosmology, J. Geom. Phys. **62**, 2401 (2012).
[42] J. P. M. Pitelli and A. Saa, Quantum singularities in Horava-Lifshitz cosmology, Phys. Rev. D **86**, 063506 (2012).
[43] B. Vakili and V. Kord, Classical and quantum Hořava-Lifshitz cosmology in a minisuperspace perspective, Gen. Relativ. Gravit. **45**, 1313 (2013).
[44] O. Obregon and J. A. Preciado, Quantum cosmology in Hořava-Lifshitz gravity, Phys. Rev. D **86**, 063502 (2012).
[45] D. Benedetti and J. Henson, Spacetime condensation in $(2+1)$-dimensional CDT from a Hořava–Lifshitz minisuperspace model, Classical Quantum Gravity **32**, 215007 (2015).
[46] H. García-Compeán and D. Mata-Pacheco, Lorentzian vacuum transitions in Hořava-Lifshitz gravity, Universe **8**, 237 (2022).
[47] A. Wang, Hořava gravity at a Lifshitz point: A progress report, Int. J. Mod. Phys. D **26**, 1730014 (2017).
[48] M. Herrero-Valea, The status of Hořava gravity, Eur. Phys. J. Plus **138**, 968 (2023).
[49] A. Emir Gümrükçüoğlu, M. Saravani, and T. P. Sotiriou, Hořava gravity after GW170817, Phys. Rev. D **97**, 024032 (2018).
[50] O. Ramos and E. Barausse, Constraints on Hořava gravity from binary black hole observations, Phys. Rev. D **99**, 024034 (2019); Phys. Rev. D **104**, 069904(E) (2021).
[51] T. Gupta, M. Herrero-Valea, D. Blas, E. Barausse, N. Cornish, K. Yagi, and N. Yunes, New binary pulsar constraints on Einstein-æther theory after GW170817, Classical Quantum Gravity **38**, 195003 (2021).
[52] N. Franchini, M. Herrero-Valea, and E. Barausse, Relation between general relativity and a class of Hořava gravity theories, Phys. Rev. D **103**, 084012 (2021).
[53] R. Loll and L. Pires, Role of the extra coupling in the kinetic term in Hořava-Lifshitz gravity, Phys. Rev. D **90**, 124050 (2014).
[54] A. Kehagias and K. Sfetsos, The black hole and FRW geometries of non-relativistic gravity, Phys. Lett. B **678**, 123 (2009).
[55] N. Afshordi, Cuscuton and low energy limit of Horava-Lifshitz gravity, Phys. Rev. D **80**, 081502 (2009).
[56] S. Dutta and E. N. Saridakis, Overall observational constraints on the running parameter λ of Horava-Lifshitz gravity, J. Cosmol. Astropart. Phys. 05 (2010) 013.
[57] N. A. Nilsson, Preferred-frame effects and the H_0 tension, and probes of Hořava-Lifshitz gravity, Eur. Phys. J. Plus **135**, 361 (2020).
[58] W. Xu, λ phase transition in Horava gravity, Adv. High Energy Phys. **2018**, 2175818 (2018).
[59] E. Di Valentino, N. A. Nilsson, and M.-I. Park, A new test of dynamical dark energy models and cosmic tensions in Hořava gravity, Mon. Not. R. Astron. Soc. **519**, 5043 (2023).
[60] N. A. Nilsson and M.-I. Park, Tests of standard cosmology in Hořava gravity, Bayesian evidence for a closed universe, and the Hubble tension, Eur. Phys. J. C **82**, 873 (2022).
[61] N. Frusciante, M. Raveri, D. Vernieri, B. Hu, and A. Silvestri, Hořava gravity in the effective field theory formalism: From cosmology to observational constraints, Phys. Dark Universe **13**, 7 (2016).
[62] W. Handley, Curvature tension: Evidence for a closed universe, Phys. Rev. D **103**, L041301 (2021).
[63] T. Jacobson, Undoing the twist: The Hořava limit of Einstein-aether theory, Phys. Rev. D **89**, 081501 (2014).
[64] B. Audren, D. Blas, J. Lesgourgues, and S. Sibiryakov, Cosmological constraints on Lorentz violating dark energy, J. Cosmol. Astropart. Phys. 08 (2013) 039.
[65] G. Calcagni, Cosmology of the Lifshitz universe, J. High Energy Phys. 09 (2009) 112.
[66] E. Kiritsis and G. Kofinas, Hořava-Lifshitz cosmology, Nucl. Phys. **821**, 467 (2009).
[67] N. A. Nilsson and E. Czuchry, Hořava-Lifshitz cosmology in light of new data, Phys. Dark Universe **23C**, 100253 (2018).
[68] P. Hořava, Quantum gravity at a Lifshitz point, Phys. Rev. D **79**, 084008 (2009).
[69] A. E. Gumrukcuoglu and S. Mukohyama, Horava-Lifshitz gravity with $\lambda \to \infty$, Phys. Rev. D **83**, 124033 (2011).
[70] S. M. Carroll and E. A. Lim, Lorentz-violating vector fields slow the universe down, Phys. Rev. D **70**, 123525 (2004).
[71] S. Dutta and E. N. Saridakis, Observational constraints on Hořava-Lifshitz cosmology, J. Cosmol. Astropart. Phys. 01 (2010) 013.
[72] E. Kiritsis, Spherically symmetric solutions in modified Horava-Lifshitz gravity, Phys. Rev. D **81**, 044009 (2010).
[73] M. Henneaux, A. Kleinschmidt, and G. Lucena Gómez, A dynamical inconsistency of Horava gravity, Phys. Rev. D **81**, 064002 (2010).
[74] B. Chen, S. Pi, and J.-Z. Tang, Power spectra of scalar and tensor modes in modified Horava-Lifshitz gravity, arXiv:0910.0338.
[75] H.-T. Janka, Neutrino emission from supernovae, in *Handbook of Supernovae*, edited by A. W. Alsabti and P. Murdin (Springer International Publishing, Cham, 2017), pp. 1575–1604, arXiv:1702.08713.
[76] F. Piron, Gamma-ray bursts at high and very high energies, C.R. Phys. **17**, 617 (2016), gamma-ray astronomy/Astronomie des rayons gamma—Volume 2.
[77] J. Dunkley, M. Bucher, P. G. Ferreira, K. Moodley, and C. Skordis, Fast and reliable mcmc for cosmological parameter estimation, Mon. Not. R. Astron. Soc. **356**, 925 (2005).
[78] N. Aghanim *et al.* (Planck Collaboratioin), Planck 2018 results. VI. Cosmological parameters, Astron. Astrophys. **641**, A6 (2020); Astron. Astrophys. **652**, C4(E) (2021).
[79] S. Carneiro, P. C. de Holanda, C. Pigozzo, and F. Sobreira, Is the H_0 tension suggesting a fourth neutrino generation?, Phys. Rev. D **100**, 023505 (2019).
[80] K. Hagiwara *et al.* (Particle Data Group), Review of particle physics, Phys. Rev. D **66**, 010001 (2002).
[81] G. Steigman, Primordial nucleosynthesis: Successes and challenges, Int. J. Mod. Phys. E **15**, 1 (2006).
[82] R. H. Cyburt, B. D. Fields, K. A. Olive, and T.-H. Yeh, Big bang nucleosynthesis: 2015, Rev. Mod. Phys. **88**, 015004 (2016).

[83] E. Di Valentino, A. Melchiorri, and J. Silk, Planck evidence for a closed Universe and a possible crisis for cosmology, Nat. Astron. **4**, 196 (2019).
[84] S. Liberati, L. Maccione, and T. P. Sotiriou, Scale hierarchy in Hořava-Lifshitz gravity: Strong constraint from synchrotron radiation in the crab nebula, Phys. Rev. Lett. **109**, 151602 (2012).
[85] V. A. Kostelecky and N. Russell, Data tables for Lorentz and *CPT* violation, Rev. Mod. Phys. **83**, 11 (2011).
[86] A. V. Kostelecky and J. D. Tasson, Matter-gravity couplings and Lorentz violation, Phys. Rev. D **83**, 016013 (2011).
[87] M. Colombo and A. E. Gümrükçüoğlu, and T. P. Sotiriou, Hořava gravity with mixed derivative terms, Phys. Rev. D **91**, 044021 (2015).
[88] M. Colombo, A. E. Gümrükçüoğlu, and T. P. Sotiriou, Hořava gravity with mixed derivative terms: Power counting renormalizability with lower order dispersions, Phys. Rev. D **92**, 064037 (2015).
[89] A. Coates, M. Colombo, and A. E. Gümrükçüoğlu, and T. P. Sotiriou, Uninvited guest in mixed derivative Hořava gravity, Phys. Rev. D **94**, 084014 (2016).
[90] J. Klusoň, Hamiltonian analysis of mixed derivative Hořava-Lifshitz gravity, Phys. Rev. D **94**, 104043 (2016).
[91] W. Hu and N. Sugiyama, Small scale cosmological perturbations: An analytic approach, Astrophys. J. **471**, 542 (1996).
[92] Z. Zhai, C.-G. Park, Y. Wang, and B. Ratra, CMB distance priors revisited: Effects of dark energy dynamics, spatial curvature, primordial power spectrum, and neutrino parameters, J. Cosmol. Astropart. Phys. 07 (2020) 009.
[93] D. Scolnic *et al.*, The Pantheon + analysis: The full data set and light-curve release, Astrophys. J. **938**, 113 (2022).
[94] D. Brout *et al.*, The Pantheon + analysis: Cosmological constraints, Astrophys. J. **938**, 110 (2022).
[95] J. Liu and H. Wei, Cosmological models and gamma-ray bursts calibrated by using Pade method, Gen. Relativ. Gravit. **47**, 141 (2015).
[96] G. Ghirlanda, G. Ghisellini, and C. Firmani, Gamma ray bursts as standard candles to constrain the cosmological parameters, New J. Phys. **8**, 123 (2006).
[97] R. Jimenez and A. Loeb, Constraining cosmological parameters based on relative galaxy ages, Astrophys. J. **573**, 37 (2002).
[98] M. Moresco, L. Verde, L. Pozzetti, R. Jimenez, and A. Cimatti, New constraints on cosmological parameters and neutrino properties using the expansion rate of the Universe to $Z \sim 1.75$, J. Cosmol. Astropart. Phys. 07 (2012) 053.
[99] M. Moresco, Raising the bar: New constraints on the Hubble parameter with cosmic chronometers at $z \sim 2$, Mon. Not. R. Astron. Soc. **450**, L16 (2015).
[100] A. Gómez-Valent and L. Amendola, H_0 from cosmic chronometers and Type Ia supernovae, with Gaussian processes and the weighted polynomial regression method, in Proceedings of the 15th Marcel Grossmann Meeting on Recent Developments in Theoretical and Experimental *General Relativity*, Astrophysics, and Relativistic Field Theories (2019), arXiv:1905.04052.
[101] M. Moresco *et al.*, Unveiling the Universe with emerging cosmological probes, Living Rev. Relativity **25**, 6 (2022).
[102] M. Moresco, R. Jimenez, L. Verde, A. Cimatti, and L. Pozzetti, Setting the stage for cosmic chronometers. II. Impact of stellar population synthesis models systematics and full covariance matrix, Astrophys. J. **898**, 82 (2020).
[103] C. Blake *et al.*, The WiggleZ dark energy survey: Joint measurements of the expansion and growth history at z ¡ 1, Mon. Not. R. Astron. Soc. **425**, 405 (2012).
[104] D. J. Eisenstein and W. Hu, Baryonic features in the matter transfer function, Astrophys. J. **496**, 605 (1998).
[105] J. E. Bautista *et al.*, The completed SDSS-IV extended Baryon Oscillation Spectroscopic Survey: Measurement of the BAO and growth rate of structure of the luminous red galaxy sample from the anisotropic correlation function between redshifts 0.6 and 1, Mon. Not. R. Astron. Soc. **500**, 736 (2020).
[106] S. Alam *et al.* (BOSS Collaboration), The clustering of galaxies in the completed SDSS-III Baryon Oscillation Spectroscopic Survey: cosmological analysis of the DR12 galaxy sample, Mon. Not. R. Astron. Soc. **470**, 2617 (2017).
[107] G.-B. Zhao *et al.*, The clustering of the SDSS-IV extended Baryon Oscillation Spectroscopic Survey DR14 quasar sample: A tomographic measurement of cosmic structure growth and expansion rate based on optimal redshift weights, Mon. Not. R. Astron. Soc. **482**, 3497 (2019).
[108] J. Hou *et al.*, The completed SDSS-IV extended Baryon Oscillation Spectroscopic Survey: BAO and RSD measurements from anisotropic clustering analysis of the Quasar Sample in configuration space between redshift 0.8 and 2.2, Mon. Not. R. Astron. Soc. **500**, 1201 (2020).
[109] R. Neveux *et al.*, The completed SDSS-IV extended Baryon Oscillation Spectroscopic Survey: BAO and RSD measurements from the anisotropic power spectrum of the quasar sample between redshift 0.8 and 2.2, Mon. Not. R. Astron. Soc. **499**, 210 (2020).
[110] A. Tamone *et al.*, The completed SDSS-IV extended Baryon Oscillation Spectroscopic Survey: Growth rate of structure measurement from anisotropic clustering analysis in configuration space between redshift 0.6 and 1.1 for the Emission Line Galaxy sample, Mon. Not. R. Astron. Soc. **499**, 5527 (2020).
[111] A. de Mattia *et al.*, The completed SDSS-IV extended Baryon Oscillation Spectroscopic Survey: Measurement of the BAO and growth rate of structure of the emission line galaxy sample from the anisotropic power spectrum between redshift 0.6 and 1.1, Mon. Not. R. Astron. Soc. **501**, 5616 (2021).
[112] S. Nadathur *et al.*, The completed SDSS-IV extended baryon oscillation spectroscopic survey: Geometry and growth from the anisotropic void–galaxy correlation function in the luminous red galaxy sample, Mon. Not. R. Astron. Soc. **499**, 4140 (2020); Mon. Not. R. Astron. Soc. **516**, 2936(E) (2022).
[113] H. du Mas des Bourboux *et al.*, The completed SDSS-IV Extended Baryon Oscillation Spectroscopic Survey: Baryon acoustic oscillations with Lyα forests, Astrophys. J. **901**, 153 (2020).